






Implementation of a Testbed for GNSS-R Payload Performance Evaluation

Adrian Perez , Joan Francesc Munoz-Martin , *Member, IEEE*, Jorge Querol , *Member, IEEE*, Hyuk Park , *Senior Member, IEEE*, and Adriano Camps , *Fellow, IEEE*

Abstract—The functional performance of space-borne instruments must be validated on ground before and after satellite integration. The effects of radio-frequency interference are also becoming more important, even in protected bands for earth observation. In this article, a GNSS and GNSS-R signal simulator is developed as part of a testbed of GNSS receivers and GNSS-R payloads' performance in high dynamics, and to study the effects of RFI in the GNSS-R observables. This article describes the different concepts and key enabling techniques that have been developed to support this project.

Index Terms—Earth Observatio (EO), Global Navigation Satellite System (GNSS), GNSS-Reflectometry (GNSS-R), radio-frequency interference (RFI), simulation, software-defined radio (SDR).

I. INTRODUCTION

IN SPACEBORNE applications, the validation of flight instrumentation is critical to ensure mission success. Earth Observation (EO) techniques using Global Navigation Satellite System (GNSS) signals of opportunity such as GNSS-Reflectometry (GNSS-R) are gaining popularity in the recent years. These techniques are difficult to test due to the high cost of GNSS simulators, forcing in many cases to launch non-properly tested instruments, which then may cause a failure of the entire mission. Some commercial GNSS simulators have proven insufficient for precise navigation measurements (see Fig. 1) or to test GNSS-R payloads, as no simulators currently

Manuscript received March 5, 2020; revised April 20, 2020 and May 13, 2020; accepted May 15, 2020. Date of publication May 28, 2020; date of current version June 15, 2020. This work was supported in part by Spanish Ministerio de Ciencia, Innovación y Universidades and EU ERDF under Project RTI2018-099008-B-C21, in part by the Sensing With Pioneering Opportunistic Techniques under Grant MDM-2016-0600, in part by the Maria de Maetzu Excellence Research Units CommSensLab, and in part by Spanish Ministerio de Economía y Competitividad (MINECO/FEDER). (*Corresponding author: Adrian Perez.*)

Adrian Perez, Joan Francesc Munoz-Martin, and Adriano Camps are with CommSensLab, Unidad Maria de Maetzu, Department of Signal Theory and Communications, UPC-BarcelonaTech and IEEC/CTE-UPC, Universitat Politècnica de Catalunya 08034, Barcelona, Spain (e-mail: adrian.perez.portero@upc.edu; joan.francesc@tsc.upc.edu; camps@tsc.upc.edu).

Jorge Querol is with the Interdisciplinary Centre for Security, Reliability and Trust, University of Luxembourg 4365, Esch-sur-Alzette, Luxembourg (e-mail: jorge.querol@uni.lu).

Hyuk Park is with CommSensLab, Unidad Maria de Maetzu, Department of Signal Theory and Communications, IEEC/CTE-UPC, Universitat Politècnica de Catalunya 08034, Barcelona, Spain, and also with the Department of Physics, Castelldefels School of Telecommunications and Aerospace Engineering, UPC-BarcelonaTech 08034, Barcelona, Spain (e-mail: park.hyuk@upc.edu).

Digital Object Identifier 10.1109/JSTARS.2020.2997717

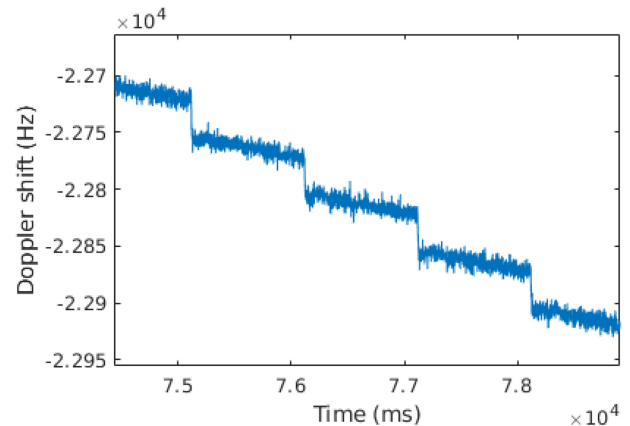


Fig. 1. Sample Doppler frequency of a GPS signal generated by a commercial GNSS signal generator, showing its granularity (50 Hz Doppler step every second).

exist for reflected signals over very large areas (e.g., ocean) and even less taking into account the Earth's curvature.

During the development of the FSSCat [1] mission, the need to test the Flexible Microwave Payload 2 (FMPL-2) [2] arose, prompting for the development of a testbed to verify GNSS signal reception, GNSS-R signals processing, and robustness against radio-frequency interference (RFI). In order to test GPS signal reception with configurable scenarios, a GPS signal generator was developed with the capability to simulate navigation (NAV) messages to allow positioning, as well as simulating any user-defined path with real GPS satellite handovers. During the development of this signal generator, an upgrade to generate also signals reflected off the earth surface was subsequently implemented. This upgrade bestowed the signal generator with the capability to simulate specular and scattered reflections to test the delay-Doppler map (DDM) calculations in the FMPL-2 [3]. An example of spaceborne DDM is shown in Fig. 2. A modified version of this embedded DDM generator was also implemented to test the generated GPS signal in combination with the simulated reflection.

The use and abuse of the frequency spectrum has caused an increase in the problem of RFI. This phenomenon can appear unintentionally, or intentionally to harm existing systems. With its proliferation, RFI has become one of the most concerning topics on GNSS-based applications, not only for navigation, positioning and timing, but nowadays also for EO, such as in GNSS-R and radio occultation due to the corruption of the received signal,

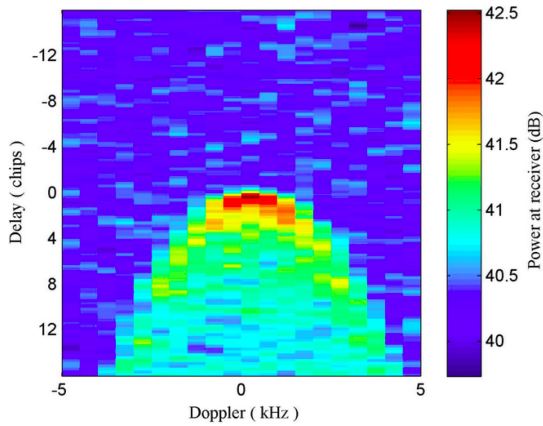


Fig. 2. DDM over the ocean measured by the U.K. TechDemoSat-1 mission.

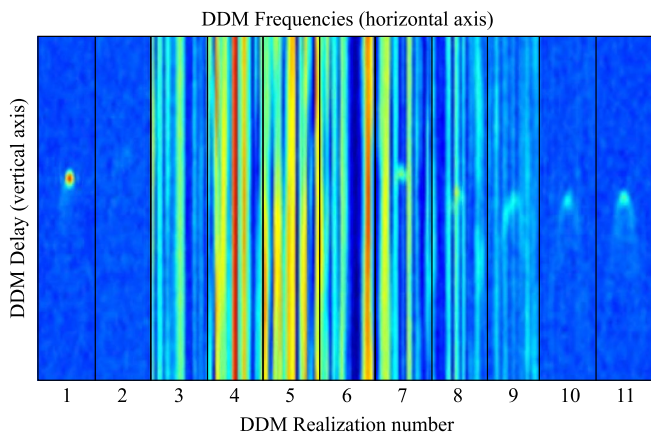


Fig. 3. Effects of RFI observed from TDS-1. The figure shows a time series of different DDMs with 10 KHz of span taken in succession, with strong RFI events destroying the observables [4].

and the corresponding geophysical measurements. Because of the difference in power, samples get totally corrupted by RFI, and recovering the original GNSS signal becomes impossible, as shown in Fig. 3. As regulations and law enforcement are often unable to control RFI, detection and mitigation techniques are becoming a must in microwave radiometry and GNSS-related missions.

The problem of RFI mitigation then involves the detection of stochastic signals with usually unknown parameters. Statistical tests, typically normality tests such as Kurtosis [5], are used to determine if a set of samples belongs to a certain statistical distribution or not. Kurtosis is a measure of the “tailedness” or “peakedness” of the probability distribution of a random variable. This means that a higher kurtosis value is the result of infrequent extreme deviations (or outliers), as opposed to frequent modestly sized deviations. Kurtosis is one of many other normality tests [6] among other RFI detection and mitigation techniques, as shown in [7]. One practical implementation of the aforementioned detection and mitigation techniques was implemented in the Front-End GNSS Interference eXcisor (FENIX) [8]. In order to test the complete system, from signal generation to the effects of RFI in the recovered signals, a hardware-in-the-loop testbed has been developed, and the results

of using this holistic approach are analyzed. The testbed consists of a signal generator that can synthesize either the direct or the reflected GNSS signals, which are then transmitted using a software-defined radio (SDR). These signals are fed into the systems under test, allowing for the validation of the implementation and its performance. After measuring the effects of RFI in the aforementioned systems, the FENIX can be introduced as a plug-and-play solution, and its capabilities as an RFI mitigator are assessed for various applications.

In this article, the implementation of the testbed and the test procedures will be explained. In Section II, the method for generating direct and reflected signals is described in detail, considering both the specular and scattered reflection cases. The testing procedure and the results are presented in Section III, followed by the conclusions.

II. GNSS SIGNAL GENERATOR

In order to test GNSS receivers in high dynamics conditions (i.e., low Earth orbit (LEO), height of 400–600 km, speed ~ 7.5 km/s), specialized equipment such as the Rohde and Schwarz SMU200A [9] with the high dynamics add-on (SMU-K77), the Spirent GSS6700 [10], etc., can be used to generate the signals that are then fed to the payloads for testing. During previous test campaigns, it was shown that even some professional equipment was unable to generate signals with enough granularity to allow for the correct testing of very specific procedures, such as filter bandwidth optimization for high dynamics environments. The cost of newer GNSS signal generators can be very expensive, which makes them prohibitive for small institutions or universities.

This prompted the design and implementation of an in-house GPS simulator that could be executed in a personal computer and then transmitted using SDR hardware. In order to test in-house developed GPS receivers and GNSS-R payloads with this software, the following requirements were set.

- 1) At least GPS L1 C/A Signal shall be generated.
- 2) Valid Ephemeris and L1 C/A NAV messages have to be transmitted so that GPS receivers can lock on the signal.
- 3) Any user-defined path (waypoints) should be able to be uploaded, either on the Earth or in orbit, with as much temporal resolution as necessary.
- 4) It shall generate both direct and reflected signals, on rough or smooth surfaces.
- 5) In the case of GNSS-R, a DDM calculator plus visualizer shall be developed to test the payload software.

In order to fulfill the aforementioned requirements, not only the direct signal, but also the signal reflected on the surface need to be modeled and generated. By using SDR devices, the signals can be transmitted and subsequently fed into any system under test, making this generator ubiquitous and independent.

A. GPS Synthetic Signal

For the simulation, a time frame has to be defined, and correspondingly the positions of the GPS constellation satellites can be determined. Using data downloaded from the Crustal Dynamics Data Information System (CDDIS) [11] from NASA, the

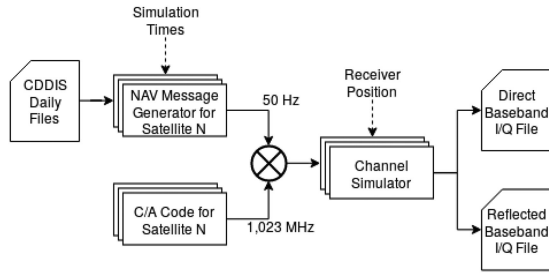


Fig. 4. Block diagram of the synthetic GPS Signal Generation.

ephemeris and almanac of a certain GPS satellite at a specified time can be reconstructed as follows.

- 1) *Ephemerides*: They contain information on week number, satellite accuracy and health, age of data, satellite clock correction coefficients, and orbital parameters. Each ephemeris is unique to a satellite.
- 2) *Almanac*: It contains less accurate orbital information than the ephemerides, and is valid for up to 90 days. It is used to speed up the time to first fix to 30 s compared to not having an almanac stored.

A GPS receiver is then capable to compute positions with the information stored in the ephemeris.

The navigation message transmitted by each satellite contains both ephemeris and almanac, and consists of five subframes of ten words each [12].

- 1) Subframes 1–3: Ephemerides.
- 2) Subframes 4–5: Almanac.

Using the daily data from CDDIS, a synthetic base-band signal can be generated by multiplexing the navigation message at 50 Hz with the C/A Codes at 1023 MHz (see Fig. 4). This results in a signal that, when modulated onto a 1575 MHz carrier and added to the signals generated by at least three other satellites, produces a GPS-like signal that receivers can lock onto.

Once the location of the transmitting satellite and the information to be transmitted are known, the signal has to be processed to account for physical effects derived from the propagation through the ionosphere, and free-space path losses. As these effects vary depending on the position of the receiver, it has to be properly defined either by a series of positions or with a two-line element (TLE) file that can be used to obtain the orbit for a given time.

B. Direct Signal Modeling

The signal directly received from the GPS is affected by the distance of the path traversed (delayed), and the relative velocity between the GPS and the receiving satellites (Doppler frequency). In this version of the test bench and for simplicity, ionospheric [13] and tropospheric [14] effects introduced by the propagation are not included.

Receivers in high dynamic environments are problematic due to the difficulty to acquire and track signals with large Doppler frequency rates. The larger the relative velocity between spacecrafts, the larger the observed Doppler frequency shift, which

can be as high as 45 kHz [15], as satellite speed increases at lower altitudes. Traditionally, loop filters are used to reduce noise and produce an accurate estimate of the original signal at its output. The loop filter order and noise bandwidth also determine the response to signal dynamics [12]. By using large bandwidths, filters are able to track signals with high Doppler rates, at the expense of introducing more noise into the system. This bandwidth is also critical while simulating GPS receivers in high dynamic environments: if the simulation steps are not small enough, Doppler frequency shifts between steps can be in the order of 50 Hz for a step of 1 s in LEO satellites (see, e.g., Fig. 1), preventing older receivers with an operating bandwidth of 1 Hz from tracking the signal at the discontinuities, forcing a new acquisition. Even for newer receivers with an operating bandwidth ranging between 20 and 50 Hz, such a discontinuity can disrupt the tracking. It is then imperative for the simulator to allow a simulation step as small as needed for the test ($\ll 1$ ms), which implies the same precision in the definition of the position of the receiver. It is important to note that ground-based and low altitude receivers should be constrained with an elevation mask of around $\geq 5^\circ$ to avoid simulating satellites that would not be in view of the receiver, whereas the elevation mask for space-borne receivers is usually around $\geq -30^\circ$ (i.e., 120° from the zenith).

Once the velocity of the transmitter and the receiver are known, for example by propagating the orbit using the Simplified General Perturbations Model with the appropriate TLE [16], the observed frequency f can be calculated as

$$f = \left(1 + \frac{\Delta v}{c}\right) f_0 = f_0 + \Delta f \quad (1)$$

where Δv is the relative velocity between the two objects, c is the speed of light, f_0 is the original transmitted frequency, and Δf is the Doppler frequency shift. It is then possible to obtain the Doppler shift from the position of the transmitter and receiver over time as

$$\Delta f = -\frac{1}{\lambda} \frac{\partial |\Delta \vec{r}|}{\partial t}. \quad (2)$$

The obtained Δf is then used to shift the carrier frequency of the GPS signal to simulate the dynamics of the receiver. Using the distance between the two objects $\Delta \vec{r}(t)$, a delay corresponding to the propagation of the signal in space $\Delta \tau = |\Delta \vec{r}(t)|/c$ can be added to the navigation message to simulate the path traversed.

C. Reflected Signal Modeling

In GNSS-R, the reflection of GNSS signals on the earth's surface is used to extract physical parameters (e.g., [17], [18]). These reflected signals clearly differ from the direct case: the distance travelled is larger, scattering can take place on multiple facets of the surface (i.e., multipath), and the signal itself is modified by the properties of the surface [19]. In a smooth surface such as a calm sea, or ice, the reflection looks like that of a mirror-like surface: the right-handed circular polarization changes to left-handed, the reflection comes from a small region around the specular reflection point (first Fresnel zone) [20] and

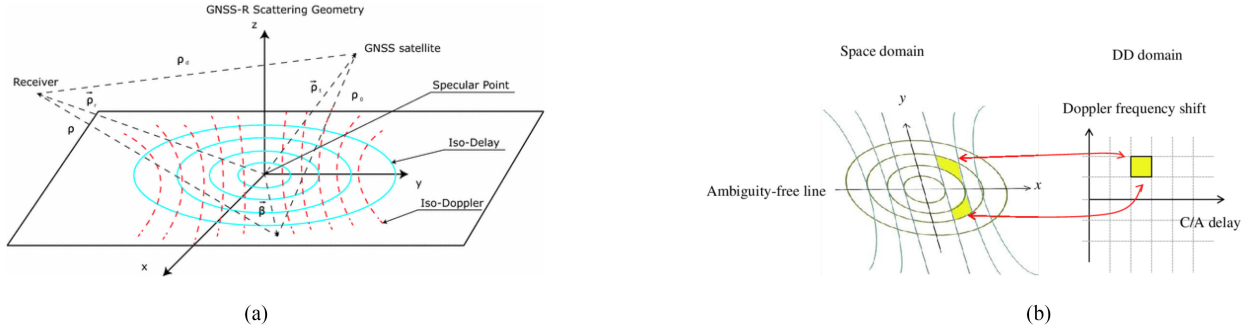


Fig. 5. Relationship between the effects of scattering and the observed DDM. (a) Geometry of the scattered signal over a rough surface. (b) Mapping between a signal footprint on a rough sea surface and its corresponding delay-Doppler observable.

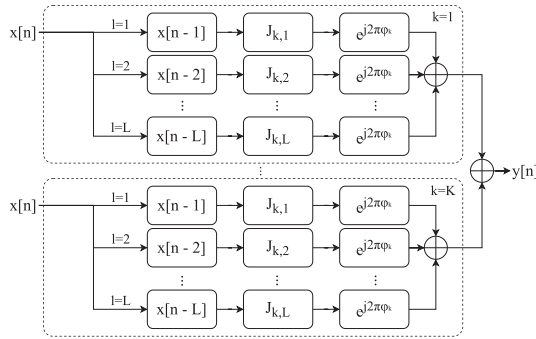


Fig. 6. Graphical representation of the filter bank used to generate the scattered signal $y[n]$ from the specular reflected signal $x[n]$.

the signal is scaled and phase shifted by the reflection coefficient of the surface.

To simulate this, the specular point of the reflection of the signal on the earth's surface must be precisely calculated. The original script in Gleason *et al.* [24] converted to the C programming language for performance, and upgraded with the BLAS library [21] to accelerate it. Further details on this algorithm can be found in Appendix A.

With this new specular point, the path for the reflected signal can be created, and then be used to calculate the new delay for the reflected signal, as performed in Section II-B. The Doppler frequency shift for the reflected path can be calculated as

$$\Delta f_{\text{REF}} = -\frac{1}{\lambda} \left\{ \frac{\partial |\Delta \vec{r}_{T-S}|}{\partial t} + \frac{\partial |\Delta \vec{r}_{S-R}|}{\partial t} \right\} \quad (3)$$

where $\Delta \vec{r}_{T-S}$ is the relative distance between the transmitter \mathbf{T} and the specular point \mathbf{S} , and $\Delta \vec{r}_{S-R}$ is the relative distance between the specular point \mathbf{S} and the receiver \mathbf{R} . In a similar manner to the previous case, the receiver should be constrained with an elevation mask to avoid unwanted paths.

D. Scattered Reflection on a Rough Surface

When the signal is reflected on a nonsmooth surface such as a rough sea, a combination of reflections appear from higher Fresnel zones further away from the specular reflection point [see Fig. 5(a)]. As shown in Fig. 5(b), there is a mapping between the different reflection zones and the frequency shifts in delay and Doppler of the received signal [22]. Note also that, except

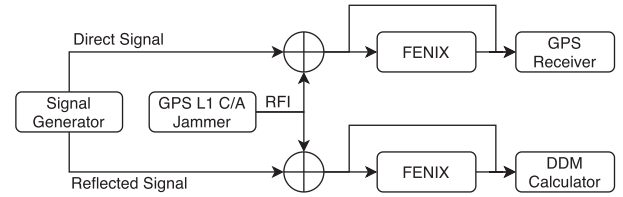


Fig. 7. Testbed for GNSS and GNSS-R Payloads, including performance characterization of the FENIX system.

for the specular reflection point, the mapping is ambiguous, i.e., one point in the DDM corresponds to two points in the spatial domain. To simulate this effect, a delay-Doppler space in agreement with the desired resolution in both domains is created. By using a derivation of the explicit expression of the space coordinates as a function of the delay offset and Doppler shift, the area for each reflection can be calculated, and thus, the power needed to be injected at each bin to obtain the simulated physical parameters. As explained in [22] and [23], the use of a change of variables between space and delay-Doppler domains allows for an efficient simulation in the latter domain of a physical measurement in the former. This is modeled as a filter bank with coefficients obtained from the Jacobian change of variables, thus producing a signal that when processed, the characteristic horseshoe [24] can be obtained in the DDM. The filter bank can be understood as

$$y[n] = \sum_{i \in \Delta f} \sum_{j \in \tau} \mathbf{J}_{ij} \cdot x[n-j] \cdot e^{j2\pi\phi_i} \quad (4)$$

where Δf are the different iso-Doppler lines, τ are the iso-delay lines, \mathbf{J}_{ij} is the coefficient from the Jacobian matrix associated to the aforementioned iso-delay and iso-Doppler lines in the space domain, $x[n]$ is the synthetic GPS signal, and

$$\phi_i = \omega_0 \cdot \tau + \varphi_{\Gamma} \quad (5)$$

is the phase of the signal at the receiver after propagation $\omega_0 \cdot \tau$ plus the phase induced by the reflection coefficient φ_{Γ} . φ_{Γ} represents the coherency of the reflected surface in terms of carrier phase, indicating the roughness of the surface. Depending on the value selected here, the coherency of the signal will be higher (i.e., a $[0, 2\pi]$ uniform random variable φ_{Γ} means a very rough surface, while a constant φ_{Γ} , a flat surface). For low altitudes, as individual waves can be distinguished, the instantaneous wave

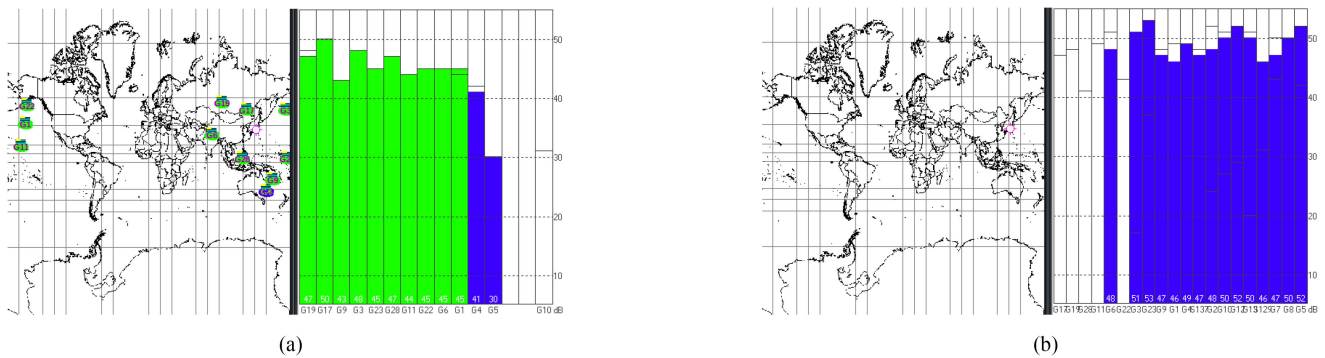


Fig. 8. Effects of RFI on the uBlox LEA-6S GNSS Receiver's C/N0. The green color indicates the C/N0 of a locked signal, whereas the blue color indicates that no lock has been achieved for that satellite. (a) Successful acquisition of lock under normal conditions. (b) Erroneous C/N0 calculation caused by RFI, thus hindering positioning.

height must be considered in order to properly model this random variable [25]. In this version of the simulator, φ_T as observed from a high-altitude receiver becomes a uniformly-distributed random variable between 0 and 2π . Appendix B provides a more detailed description of the implementation of this method capable to generate the power at each bin from a set of physical measurements that the synthetic signal is meant to represent.

The final signal, $y[n]$, is then recorded to a file as baseband I/Q samples that can then be transmitted using SDR devices, allowing for seamless integration into any system.

III. TESTBED FOR GNSS-R PAYLOADS

With the availability of this novel method to generate both GNSS and GNSS-R signals, a testbed was prepared to observe the behavior of several systems when fed with them.

The testbed described in Fig. 7 was devised to demonstrate the FENIX system [8] for RFI mitigation, as well as to explore the effects of jamming on the end systems. This configuration was presented in the inLab Session of GNSS+R 2019. Two separate paths for the direct and reflected signals were prepared with a hardware-in-the-loop approach; one to test GPS receivers, and the other to test GNSS-R equipment similar to the one in the FSSCat mission [26].

Using the process described in Section II and the data from [11], a 30-min simulation was created with a synthetic position in Japan at an arbitrary date in the past. The direct and reflected raw I/Q files were then fed to two SDRs that upconverted the signal to the GPS L1 band, as shown in Fig. 7, and several GNSS and GNSS-R experiments were conducted to illustrate the performance.

A. GNSS Testing

In the case of the direct signal, a low dynamics environment was prepared to properly explore the most common use cases, including verification of the synthetic signal and testing spoofing countermeasures.

1) *Navigation With GPS Receivers*: This test was performed using a uBlox LEA-6S receiver, both as a proof of operation and to test if the spoofing countermeasures found in commercial receivers would allow positioning from a synthetic signal.

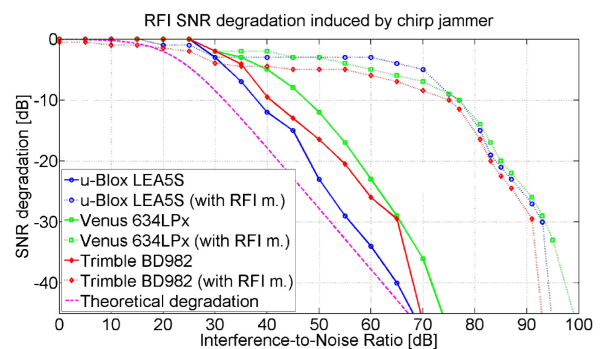


Fig. 9. Sample SNR Degradation before (solid line) and after the addition of the FENIX [27] (dashed line).

The commercial receiver was able to lock to all the simulated satellites and achieve positioning within 30 s. The output of the simulator was calibrated to match typical C/N0 values for the different satellites depending on their distance, and the receiver correctly identified as valid the 10 satellites with an elevation within line of sight, as shown in Fig. 8(a).

2) *Characterization of GNSS Receivers' Resiliency Against RFI*: This test was based on the generation of multiple jamming signals to test the capabilities of each receiver against RFI including, but not limited to, the modification of the power and shape.

The jamming signals were first introduced as an addition to the baseband simulated signal, using GNURadio to generate different RFI such as continuous waves (CWs) and chirp signals. The performance of the GNSS receivers was degraded more and more as the RFI power increased, as shown in Fig. 8(b). A commercial GPS Jammer was introduced and added to the output of the SDR to further prove the plug-and-play nature of the testbed, which allowed for multiple elements to be added to increase the likeness of the complete system to a real scenario. The commercial jammer also severely degraded the performance of the receivers, which after characterization prompted for the addition of a mitigation system. By using the FENIX [27] in the testbed architecture, right before the GPS receiver, the effects of the RFI were greatly mitigated, as shown in Fig. 9, both for the case of the CW and the chirp signals. For example,

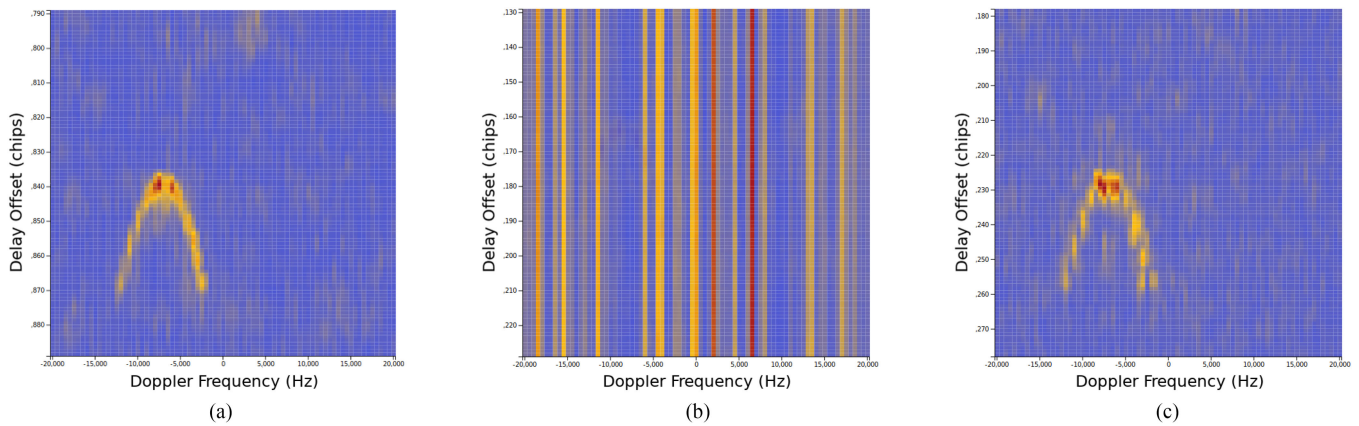


Fig. 10. Effects of simulated RFI on the synthetic DDM GNSS-R observables [27]. (a) DDM calculated from the synthetic reflected signal. Doppler frequency and Delay spreads match with the simulation parameters. (b) DDM of the signal with a high-power (10 dB INR) CW RFI centered at L1 Band. (c) DDM of the signal in Fig. 10(b) after RFI mitigation with the FENIX.

for an interference-to-noise ratio (INR) of 60 dB, the u-Blox LEA5S suffered a SNR degradation of 34 dB, whereas after the addition of the FENIX, this degradation did not exceed 4 dB. This means that the gain obtained from the mitigation scheme is approximately 30 dB.

B. GNSS-R Testing

Regarding the reflected signal, a high dynamics environment was used in the testbed to demonstrate realistic scenarios encountered while testing space-borne GNSS-R payloads. These scenarios include the computation of GNSS-R observables such as DDMs and the characterization of the effects of RFI on GNSS-R observables, similar to the ones found in TDS-1 (see Fig. 3).

1) *Computation of DDMs From the Synthetic Signal:* In order to calculate DDMs from the received reflected signal, a search has to be conducted for several GNSS C/A codes with different delays and Doppler shifts against, which the incoming signal will be correlated to.

Afterwards, the power allocated to each combination of delay and Doppler is integrated producing a matrix in the delay-Doppler space, with the power of each bin plotted as a color scale. This is called the DDM, and it can be seen in Fig. 10(a) with a delay bin resolution of 0.5 C/A chips and 80 bins of range, and a Doppler bin resolution of 500 Hz and 21 bins of range. As GPS has a code with a 1 ms chip length, 500 Hz of sampling rate are needed to detect the peak. Increasing this value dramatically increases computation time, so the sampling rate has been kept to the minimum needed.

Testing this kind of architecture realistically with the signal generator was one of the main objectives of the testbed. A satellite receiver at 700 km of height and 65° of elevation (similar to TechDemoSat-1) was simulated, and the reflected path signal was fed into the same software DDM calculator as the one used in the FSSCat mission.

The DDMs calculated from the synthetic signal bear a strong resemblance to those obtained from the TDS-1 mission [see

Figs. 2 and 10(a)], with very similar delay and Doppler frequency spreads. With this setup, the DDM calculator could be verified, and even compared to the results obtained from TDS-1.

2) *Effects of RFI on GNSS-R Observables:* Finally, the effect of RFI on GNSS-R observables was tested with a similar methodology than in Section III-A2. Introducing a CW signal (to compare with the RFI found in TDS-1, Fig. 3) corrupting the simulated reflection causes vertical (i.e., along the same frequency) glitches, as shown in Fig. 10(b), thus making it impossible to extract any physical parameter from the characteristics of the DDM. By using a specially tailored FENIX for GNSS-R, and inserting it prior to the software-based DDM calculator, a noticeable improvement in the quality of the observable can be achieved, as shown in Fig. 10(c), making it possible to extract physical measurements.

IV. CONCLUSION

Recently, GNSS and GNSS-R payloads are being selected for many small satellite missions. In this article, an efficient and cost-effective method to test, demonstrate and validate GNSS/GNSS-R payloads has been presented. Several tests performed show good results simulating GNSS signals and their corresponding DDMs. Furthermore, it helps illustrate the impact of RFI in the DDMs and consequently the performance of RFI mitigation devices.

This testbed has become a key enabling technology to test a number of GNSS and GNSS-R equipment and payloads for CubeSat missions, as well as other measurement campaigns.

As further work, the algorithms used for synthetic signal generation including the addition of ionospheric and tropospheric effects, as well as the extension of this system to other GNSSs such as Galileo or BeiDou, will allow for more realistic testing environments with a wider range of use cases. One of such cases could be the validation of GPS L5-based instruments for the acquisition of centimeter-accuracy altimetry [28].

APPENDICES

REFERENCES

A. Specular Point Calculation

The calculation of the point where the specular reflection of the signal between a spaceborne transmitter (i.e., GPS satellite) and a receiver occurs is an iterative process involving the position of both entities and the geodesy of the Earth [24].

This process implies creating a new reference frame that includes the World Geodetic System 1984 (WGS84) ellipsoid [29], and the transmitting \mathbf{T} and receiving \mathbf{R} satellites. The specular point \mathbf{S} is located at the surface of the WGS84 ellipsoid, where the angles from the rays traced between each satellite (transmitter and receiver) and the surface normal at the point are equal. An iterative approach is used to find this point, until the difference between angles is negligible.

An initial tentative point \mathbf{S}_{temp} is placed on the surface of the earth, right below the receiver \mathbf{R} . Using the unit vectors $\widehat{\mathbf{SR}}$ and $\widehat{\mathbf{ST}}$ understood as the distance traversed between the tentative point and both receiver and transmitter, the error can be obtained as the distance to the shortest path. Moving the specular point an arbitrary amount (variable gain) and repeating the process will iteratively converge to find the location of the reflection for the shortest path.

Newer versions of this method [30] will be researched to improve the performance of the signal generator to aim for real-time generation.

B. Mapping the Delay-Doppler Space to Their Physical Counterparts

In order to modify the specular reflected signal to produce an accurate DDM of a scattered reflection, the contributions from the different paths around the specular point must be understood.

The complete reflection over the scattering surface consists on the significant signal contributions over each facet in the (x, y) domain. When calculating the DDM, a more coarse grid in the $(\tau, \Delta f)$ domain is used, linked to a given surface coordinate (and all the contributions within) through a geometrical relationship

$$\begin{cases} \tau_{xy} = \tau(x, y) \\ \Delta f_{xy} = \Delta f(x, y). \end{cases} \quad (6)$$

Each point in the surface ρ then becomes

$$\rho = |J(\tau_{xy}, \Delta f_{xy})| \cdot d\Delta f_{xy} \cdot d\tau_{xy} \quad (7)$$

where $d\Delta f_{xy}$ and $d\tau_{xy}$ are the differentials of the new integration variables, and $|J|$ stands for the absolute value of the Jacobian of the change of variables defined in (6).

The Jacobian then takes into account the area associated to a given $(\tau, \Delta f)$ bin in the (x, y) domain, but this mapping is ambiguous, as shown in Fig. 5: a single $(\tau, \Delta f)$ bin corresponds to two points in the (x, y) domain, and the contribution to each of them must be taken into account.

A more extensive study on this mapping can be found in [22] and [23].

- [1] A. Camps *et al.*, "FSSCAT, the 2017 copernicus masters, "ESA sentinel small satellite challenge" winner: A federated polar and soil moisture tandem mission based on 6u cubesats," in *Proc. IEEE Int. Geosci. Remote Sens. Symp.*, Jul. 2018, pp. 8285–8287.
- [2] J. F. Munoz-Martin, L. Fernandez, J. Ruiz-de-Azua, and A. Camps, "The flexible microwave payload -2: Design, implementation, and optimization of a GNSS-R and radiometry processor for CubeSat-based earth observation missions," in *Proc. IEEE Int. Geosci. Remote Sens. Symp.*, Jul. 2019, pp. 5248–5251.
- [3] J. F. Munoz-Martin, L. F. Capon, J. A. Ruiz-de-Azua, and A. Camps, "The flexible microwave Payload-2: A SDR-based GNSS-reflectometer and L-band radiometer for CubeSats," *IEEE J. Sel. Topics Appl. Earth Observ. Remote Sens.*, vol. 13, pp. 1298–1311, Mar. 2020, doi: [10.1109/JS-TARS.2020.2977959](https://doi.org/10.1109/JS-TARS.2020.2977959).
- [4] M. Unwin, "TechDemoSat-1 and the GNSS reflectometry experiment," in *Proc. GNSS+R*, 2015.
- [5] R. De Roo, S. Misra, and C. Ruf, "Sensitivity of the kurtosis statistic as a detector of pulsed sinusoidal radio frequency interference in a microwave radiometer receiver," *IEEE Int. Geosci. Remote Sens. Symp., Barcelona*, 2007, pp. 2706–2709, doi: [10.1109/IGARSS.2007.4423401](https://doi.org/10.1109/IGARSS.2007.4423401).
- [6] J. Tarongi and A. Camps, "Normality analysis for RFI detection in microwave radiometry," *Remote Sens.*, vol. 2, pp. 191–210, Dec. 2009.
- [7] J. Querol, A. Perez, and A. Camps, "A review of RFI mitigation techniques in microwave radiometry," *Remote Sens.* vol. 11, 2019, Art. no. 3042.
- [8] "FENIX Patent," 2019. [Online]. Available: <https://patents.google.com/patent/US9596610>
- [9] "R&S SMU200A Vector Signal Generator," 2019. [Online]. Available: https://www.rohde-schwarz.com/us/product/smu200a-productstartpage_63493%20-7555.html
- [10] "Spirent," 2019. [Online]. Available: <https://www.spirent.com/go/what-is-a-gps-simulator>
- [11] "NASA Crustal Dynamics Data Information System," 2019. [Online]. Available: <https://cddis.nasa.gov/>
- [12] E. D. Kaplan and C. Hegarty, *Underst. GPS: Princ. And Appl.*, vol. 11. Norwood, MA, USA: Artech House, 2005.
- [13] A. Camps *et al.*, "Improved modelling of ionospheric disturbances for remote sensing and navigation," in *Proc. IEEE Int. Geosci. Remote Sens. Symp.*, Jul. 2017, pp. 2682–2685.
- [14] H. D. Black and A. Eisner, "Correcting satellite doppler data for tropospheric effects," *J. Geophysical Res., Atmospheres*, vol. 89, no. D2, pp. 2616–2626, 1984. [Online]. Available: <https://agupubs.onlinelibrary.wiley.com/doi/abs/10.1029/JD089iD02p02616>
- [15] A. Birklykke, "High dynamic GPS signal acquisition: A case study in GPS receivers on nano-satellites in LEO," Ph.D. dissertation, Faculties Eng., Sci. Medicine Dept. Elect. Syst., Aalborg Univ., Aalborg, Denmark, 2010.
- [16] F. R. Hoots and R. L. Roehrich, "Spacetrack report no. 3-models for propagation of norad element sets. project spacetrack reports," 1988. [Online]. Available: <https://www.celestrak.com/NORAD/documentation/spacetrk.pdf>
- [17] A. Alonso-Arroyo, V. Zavorotny, and A. Camps, "Sea ice detection using U.K. TDS-1 GNSS-R data," *IEEE Trans. Geosci. Remote Sens.*, vol. 55, no. 9, pp. 4989–5001, Sep. 2017.
- [18] E. Valencia, A. Camps, N. Rodriguez Alvarez, H. Park, and I. Ramos-Perez, "Using GNSS-R imaging of the ocean surface for oil slick detection," *IEEE J. Sel. Topics Appl. Earth Observ. Remote Sens.*, vol. 6, no. 1, pp. 217–223, Feb. 2013.
- [19] V. U. Zavorotny, S. Gleason, E. Cardellach, and A. Camps, "Tutorial on remote sensing using GNSS bistatic radar of opportunity," *IEEE Geosci. Remote Sens. Mag.*, vol. 2, no. 4, pp. 8–45, Dec. 2014.
- [20] A. Camps, "Spatial resolution in GNSS-R under coherent scattering," *IEEE Geosci. Remote Sens. Lett.*, vol. 17, no. 1, pp. 32–36, Jan. 2020.
- [21] "BLAS (Basic Linear Algebra Subprograms)," 2019. [Online]. Available: <http://www.netlib.org/blas/index.html>
- [22] J. F. Marchan-Hernandez, A. Camps, N. Rodriguez-Alvarez, E. Valencia, X. Bosch-Lluis, and I. Ramos-Perez, "An efficient algorithm to the simulation of delay-doppler maps of reflected global navigation satellite system signals," *IEEE Trans. Geosci. Remote Sens.*, vol. 47, no. 8, pp. 2733–2740, Aug. 2009.
- [23] H. Park *et al.*, "A generic level 1 simulator for spaceborne GNSS-R missions and application to GEROS-ISS ocean reflectometry," *IEEE J. Sel. Topics Appl. Earth Observ. Remote Sens.*, vol. 10, no. 10, pp. 4645–4659, Oct. 2017.

- [24] S. Gleason, D. Gebre-Egziabher, and D. Gebre Egziabher, *GNSS Appl. and Meth.*, vol. 7. Norwood, MA, USA: Artech House 2009.
- [25] J. Miranda, A. Camps, J. Gomez, M. Vall-Ilossera, and R. Villarino, "Time-dependent sea surface numerical generation for remote sensing applications," in *Proc. IEEE Int. Geosci. Remote Sens. Symp.*, 2005, vol. 4, pp. 2527–2530.
- [26] J. F. Muñoz-Martin, L. Fernandez, J. Ruiz-de-Azua, and A. Camps, "The flexible microwave payload -2: Architecture and testing of a combined GNSS-R and L-band radiometer with RFI mitigation payload for cubesat-based earth observation missions," in *Proc. IEEE Int. Geosci. Remote Sens. Symp.*, Jul. 2019, pp. 5185–5188.
- [27] A. Perez, A. Camps, and J. Querol, "On the new architecture and capabilities of the front-end GNSS interference excisor (FENIX)," in *Proc. IEEE Int. Geosci. Remote Sens. Symp.*, Jul. 2019, pp. 5163–5166.
- [28] F. Fabra *et al.*, "Is accurate synoptic altimetry achievable by means of interferometric GNSS-R?" *Remote Sens.*, vol. 11, Mar. 2019, Art. no. 505.
- [29] "NGA Geomatics - WGS84," 2019. [Online]. Available: [http://earth-info.nga.mil/GandG/update/index.php?dir=wgs84&action=wgs84%](http://earth-info.nga.mil/GandG/update/index.php?dir=wgs84&action=wgs84%20)
- [30] B. Southwell and A. Dempster, "A new approach to determine the specular point of forward reflected GNSS signals," *IEEE J. Sel. Topics Appl. Earth Observ. Remote Sens.*, vol. 11, no. 2, pp. 639–646, Feb. 2018.

Adrian Perez was born in Barcelona in 1992. He received the M.Sc. degree in telecommunications engineering in 2019, from the Universitat Politècnica de Catalunya - UPCBarcelonaTech, Barcelona, Spain, where he is currently working towards a doctoral degree in the field of radio frequency interference and signal processing.

He joined the NanoSat-Lab in 2018 as a Software Engineer, working on several projects related to GNSS technologies, such as RFI Mitigation and GNSS-R Simulation. He is currently participating in the ³Cat-4 and ESA S³ FSSCat mission as Software, Ground Segment, and Operations Engineer. He is also currently working on the FENIX (Front-End GNSS Interference eXcisor) and other RFI detection products, as well as in the RITA payload, winner of the second GRSS Student Challenge.

Joan Francesc Muñoz-Martin (Member, IEEE) was born in Mallorca in 1992. He received the M.Sc. degree in telecommunications engineering from the Universitat Politècnica de Catalunya, Barcelona, Spain, in 2017, where he is currently working toward the doctoral degree in advanced GNSS-R receivers for nanosatellites.

He joined the NanoSat Lab in 2013 as a Communications System Engineer for the 3Cat-1 mission and has been involved in all its missions ever since. He participated in ESA's BEXUS 19 and led the OBDH, TT&C, and Ground Operations for 3Cat-2 mission. As part of his doctoral degree, he participates in 3Cat-4 and ESA S³ FSSCat mission. He is the Lead Software and Payload Engineer for the FMPL-1, and the Payload Manager of FMPL-2, the GNSS-R and radiometry microwave passive payloads of 3Cat-4 and FSSCat, respectively. He is also part of the science team of the GNSS-R experiment carried in the MOSAiC campaign in the Arctic Sea.

Jorge Querol (Member, IEEE) was born in Forcall, Castelló, Spain, in 1987. He received the B.Sc. (+5) degree in telecommunication engineering, the M.Sc. degree in electronics engineering, the M.Sc. degree in photonics, and the Ph.D. degree (*Cum Laude*) in signal processing and communications from the Universitat Politècnica de Catalunya - BarcelonaTech (UPC), Barcelona, Spain, in 2011, 2012, 2013, and 2018, respectively.

His Ph.D. thesis was devoted to the development of novel antijamming and counter-interference systems for Global Navigation Satellite Systems (GNSS), GNSS-Reflectometry, and microwave radiometry. One of his outstanding achievements was the development of a real-time standalone precorrelation mitigation system for GNSS, named FENIX, in a customized SDR platform. FENIX was patented, licensed, and commercialized by MITIC Solutions, a UPC spin-off company. Since 2018, he is Research Associate with the SIGCOM research group of the Interdisciplinary Centre for Security, Reliability, and Trust (SnT) of the University of Luxembourg, Luxembourg. He is involved in several ESA and Luxembourgish national research projects dealing with signal processing and satellite communications. His research interests include SDR, real-time signal processing, satellite communications, 5G nonterrestrial networks, satellite navigation, and remote sensing.

Dr. Querol was the Recipient of the Best Academic Record Award of the Year in Electronics Engineering at UPC in 2012, the First Prize of the European Satellite Navigation Competition Barcelona Challenge from the European GNSS Agency in 2015, the Best Innovative Project of the Market Assessment Program of EADA Business School in 2016, the award Isabel P. Trabal from Fundació Caixa d'Enginyers for its quality research during his Ph.D. in 2017, and the Best Ph.D. Thesis Award in remote sensing in Spain from the IEEE GEOSCIENCE AND REMOTE SENSING Spanish Chapter in 2019.

Hyuk Park (Senior Member, IEEE) was born in South Korea. He received the B.S. degree in mechanical engineering from the Korea Advanced Institute of Science and Technology, Daejeon, South Korea, in 2001, and the M.S. and Ph.D. degrees in information and mechatronics from the Gwangju Institute of Science and Technology, Gwangju, South Korea, in 2003 and 2009, respectively.

In 2009, he joined the remote sensing group of the Polytechnic University of Catalonia, Barcelona, as a Postdoctoral Researcher. His main research interest include the area of remote sensing, especially passive microwave remote sensing, including system design, modeling and simulation, and image processing.

Prof. Park is a Grant Holder of NRF funded by the Korean government in 2011. In 2012–2014, he has worked as a Juan de la Cierva Researcher funded by Spanish Ministry of Science and Innovation. He is currently working with the School of Telecom. and Aerospace Engineering, RSLab, Universitat Politècnica de Catalunya as a Ramon y Cajal Fellow/Tenure-track Assistant Professor.

Adriano Camps (Fellow, IEEE) was born in Barcelona, Spain, in 1969. He received the degree in telecommunications engineering and the Ph.D. degree in telecommunications engineering from the Universitat Politècnica de Catalunya (UPC), Barcelona, Spain, in 1992 and 1996, respectively.

From 1991 to 1992, he was with the ENS des Telecommunications de Bretagne, France, with an Erasmus Fellowship. Since 1993, he has been with the Electromagnetics and Photonics Engineering Group, Department of Signal Theory and Communications, UPC, where he was an Assistant Professor first, an Associate Professor in 1997, and has been a Full Professor since 2007. In 1999, he was on sabbatical leave at the Microwave Remote Sensing Laboratory, University of Massachusetts, Amherst, MA, USA. He has been deeply involved in the European Space Agency SMOS Earth Explorer Mission, from the instrument and algorithmic points of view, performing field experiments and more recently studying the use of global navigation satellite systems reflectometry (GNSS-R) techniques to perform the sea state correction needed to retrieve salinity from radiometric observations. His research interests include microwave remote sensing, with special emphasis in microwave radiometry by aperture synthesis techniques, remote sensing using signals of opportunity (GNSS-R), and the development of nanosatellites to test innovative remote sensing techniques.